First-principles estimation of electronic structure of uranium oxychalcogenides UOY, Y = S, Se, Te. Application to the INS spectra of UOS

2000 J. Phys.: Condens. Matter 12 415

(http://iopscience.iop.org/0953-8984/12/4/305)

J. Phys.: Condens. Matter **12** (2000) 415–437. Printed in the UK PII: S0953-8984(00)05383-2

First-principles estimation of electronic structure of uranium oxychalcogenides UOY, Y = S, Se, Te. Application to the INS spectra of UOS

Z Gajek

Instytut Niskich Temperatur i Badań Strukturalnych, Polska Akademia Nauk, Skr. Poczt. 1410, 50-950 Wrocław 2, Poland

E-mail: gajek@int.pan.wroc.pl

Received 26 May 1999

Abstract. A consistent description of the electronic structure of the $U^{4+}(5f^2)$ ion in the UOY (Y = S, Se, Te) compounds derived on the basis of a model first-principles calculation is presented. The crystal field potential is discussed in detail. Special attention is paid to contributions of non-equivalent ligand groups. Their competition and variation along the series explain apparently random total values of the crystal field parameters (CFPs). Discussion of an interplay of factors dependent on the coordination geometry and so called 'intrinsic parameters' describing the separated metal–ligand (ML) linear ligators points to presumably rational ranges of actual values of CFP. Contrary to some earlier findings, the calculations evidence an approximate axial character of the crystal field potential.

A dependence of the intrinsic parameters on the ML distance is examined thoroughly. The new numerical data show a dependence weaker than that reported before. At small ML distances, the intrinsic parameters behave in a manner characteristic of the metallic state.

Some simplifications of the common phenomenological models suggested on the basis of the *ab initio* calculations open new possibilities of interpretation of complex magnetic and other properties of UOY. The obtained eigenstates of the uranium ion and simulated temperature characteristics of such quantities as the magnetic susceptibility or heat capacity may serve as good reference data.

The crystal field (CF) parameters estimated from first principles have been used as starting data in the conventional phenomenological description of the recent inelastic neutron scattering (INS) data reported for UOS by Amoretti *et al*. In contrast to the earlier phenomenological approaches the effect of the term mixing has been taken into account. In initial steps of the fitting of the INS transition energies, a variation of the CF parameters has been restricted by using the angular overlap model. Then, the CF parameters have been refined to reproduce not only the observed energies of the INS transitions but also their relative intensities and the magnitude of the ordered magnetic moment. Other measurable quantities such as the temperature dependences of magnetic susceptibility or the Schottky contribution to the heat capacity restored according to the proposed CF model have been shown to agree satisfactorily with the corresponding experimental data. The CF scheme inferred here for UOS differs essentially from that proposed by Amoretti *et al*. However, the latter, recalculated in an extended function basis allowing for the term mixing, has been demonstrated to be not convergent with the original findings.

1. Introduction

Observation of the anti-ferromagnetic long-range order in UOTe in 1961 [1] initiated a growing interest in investigation of the light actinide oxychalcogenides. Since then considerable experimental work has been done for a wide family of ternary AnXY compounds, where

0953-8984/00/040415+23$30.00

An = U, Np, X = O, N, Y = S, Se, Te [2–13]. The investigations have covered, among other things, the crystal structure [2–8], magnetic [2, 3, 5–7, 9–11], electric [2, 8] and thermal [5, 12] properties as well as spectroscopic properties investigated in terms of inelastic neutron scattering (INS) [11, 13] or Mössbauer spectroscopy [6].

The large spatial extent of the orbitals of the actinide 5f electrons and the proximity of their binding energy to those of valence electrons of neighbouring ions in a crystal implies a peculiar sensitivity of the physical properties to the chemical environment. The case of the compounds under consideration is especially complicated by the presence of two different actinide–ligand bonds: An^{4+}–X^{2-} bonds of more ionic character, which are characteristic of actinide dioxides [14], and An^{4+}–Y^{2-} bonds of more metallic character, which in turn are also observed in actinide dichalcogenides [15]. The interesting magnetic and related properties of the AnXY phases have been discussed in the light of various physical mechanisms involved. Direct and indirect exchange interactions, hybridization between localized 5f and valence band p electrons or Mott–Hubbard correlations have been considered [16]. Nevertheless, the ordinary crystal field (CF) effect still has a fundamental meaning in understanding the experimental data.

In the present paper, the CF effect in the UOY series is discussed on the ground of systematic, first-principles calculations. We follow a simple perturbation model that has just been employed in a recent study on UOSe [7]. The same theoretical model has been also applied, among the others, to the widely discussed UO_2 [17, 18] and to other uranium compounds [19, 20]. The results there obtained support believing that the model is adequate despite some obvious shortcomings. In particular, the model does not concern the mechanisms characteristic of the metallic state, which certainly do not disappear in semiconducting systems, like UO_2 or UOY. It is worth noting at this point, that the predictions obtained using more advanced theoretical approaches, including the methods based on the local density approximation (LDA), remain, for the time being, rather far from the experimentally observed CF effects [21, 22]. Quite recent calculations for UO_2 based on the LDA generalized for strong Coulomb correlations (LDA + U) indicate that the electron–electron correlations in the 5f band lead to the Heitler–London type of hybridization between the electronic orbitals [14]. The ionic one-electron approach adopted here after [7] and [19] stems from the group product function formalism that the electron correlations brings to the energy dependent terms in the effective perturbation Hamiltonian [23]. Since we are interested in the low energy CF levels only, the usual mean energy approach, giving the effective one-electron CF potential, is considered correct.

The AnXY compounds crystallize in the tetragonal PbFCl-type structure [10] in which the point group symmetry at the metal site is C_{4v}. The actinide ion is placed in between two coordination squares, one formed by ligands X and the other by ligands Y. The squares are twisted mutually by 90°. An additional Y ligand is placed on the C_4 axis out of the Y square. Three non-equivalent ligand groups can be distinguished: X, Y1, Y2. One of the aims of the present work is to analyse the influence of these groups on the total CF effect along the series. We will also examine how sensitive the separated metal–ligand (ML) interactions are to a variation of the ML distance. The results are employed to formulate simplified phenomenological models that may be useful in discussion of the experimental data and to generate some temperature characteristics, which can be related to the measured quantities directly.

As an example, the results are applied to verify recent interpretation of the inelastic neutron scattering (INS) spectra and some thermodynamic and magnetic properties of UOS reported elsewhere. This interesting compound has been intensively investigated in the past [8–13, 24]. Like other members of the series, UOS orders antiferromagnetically below $T_N = 55$ K with the AF III (++−−)-type arrangement with the magnetic moment of magnitude

of 2 μ_B aligned along the *c*-axis [9–11, 13, 24]. This has been confirmed in heat capacity measurements by the λ-shaped peak at 55.35 K [12] where, in addition, a broad maximum at about 250 K has been detected. The temperature dependence of the anisotropic magnetic susceptibility has been investigated on both single- and polycrystalline samples [9–11]. Recent electron transport measurements have demonstrated UOS to be a p-type semiconductor with activation energy of 67.5 meV [8]. Inelastic neutron scattering (INS) measurements at various temperatures, neutron incident energies and scattering angles have been reported by Amoretti *et al* [11, 13, 24]. Two main structures of magnetic origin at 74 meV and 83 meV with a shoulder at about 87 meV have been indicated in the spectrum recorded above the Néel temperature. Besides, it has been shown that these lines are slightly shifted in the ordered phase while the shoulder takes a form of separate line at 92 meV. The possibility of low intensity electronic excitations below 55 meV has also been suggested [13].

It is well known that the interpretation of the crystal field effect in the case of non-transparent crystals, for which the optical absorption data cannot be recorded, is a very difficult task. As many as five CF parameters being efficient for the C_{4v} point symmetry can hardly be adjusted to only a few INS transitions definitely. It is only natural that the interpretation of the CF effect in UOS may evolve as in the papers by Amoretti *et al* [11, 13]. Now we have the possibility to confront their findings with the new theoretical results.

2. Formulation of the model

The model used in this study has been inspired by the calculations developed by Newman for $PrCl_3$ [25]. The approach has already been presented in detail and applied for several actinide systems [7, 18–20]. Therefore, we confine ourselves to recall only its basic idea.

The main assumption is that electrons in a crystal occupy states strictly localized on the ions. This assumption justifies restriction of the considerations to the cluster consisting of the metal ion and surrounding nearest neighbours (ligands) regarding the rest of the crystal as a source of an external electrostatic potential acting on this cluster. The cluster can be treated as a system of weakly interacting groups of electrons localized on different ions that fulfils all assumptions of the group product function formalism [23].

The initial group product wavefunctions are built from the free-ion spin orbitals obtained with the standard self-consistent Dirac–Slater procedure. The ground and the most important excited electron configurations are taken into account explicitly. Standard projection, contraction and renormalization techniques are applied to reduce the initial wave-function space to the pure $5f^2$-configuration basis characteristic of the conventional phenomenological approach (see section 5). This procedure leads to the effective CF potential V acting on a 5f electron, which conventionally is written in parametrized form in terms of normalized spherical harmonic operators $\boldsymbol{C}_{kq}$:

$$V = \sum_{kqi} B_{kq} \boldsymbol{C}_{kq}(i). \tag{1}$$

The summation index i runs over all f electrons, $k = 2, 4, 6$, $q = -k, -k+1, \ldots, k$, B_{kq} are the CF parameters.

The perturbation approach allows one to distinguish several characteristic components of V:

$$V = V_R + V_C + V_{CR} + V_{IM}. \tag{2}$$

In the above equation, V_R represents a renormalization term due to the ligand–metal charge transfer and non-orthogonality of the free-ion wavefunctions localized on different ions. It turns

Table 1. Crystallographic and other data used in the calculations.

	UOS	UOSe	UOTe
Crystallographic data [8, 7, 3]			
Space group $P4/nmm$			
Lattice parameter			
a (nm)	0.384 50	0.390 38	0.401 41
c (nm)	0.668 50	0.698 05	0.749 40
Atom position U in 2c, O in 2a, Y in 2c			
z_U	0.199 00	0.189 26	0.170 30
z_Y	0.643 00	0.633 20	0.632 20
Ligand coordinates			
θ(O)	124.7	124.1	122.5
R(O) (nm)	0.233 79	0.235 70	0.237 85
θ(Y1)	68.8	65.8	62.5
R(Y1) (nm)	0.291 68	0.302 58	0.319 19
θ(Y2)	0.0	0.0	0.0
R(Y2) (nm)	0.296 81	0.309 89	0.349 22
Madelung energy (a.u.) at			
U^{4+}	1.341	1.294	1.211
O^{2-}	−0.873	−0.925	−1.014
Y^{2-}	−0.595	−0.539	−0.456
Binding energy of 'free-ion' valence electron (a.u.)			
U^{4+}: $\varepsilon_{5f} = -1.492$			
O^{2-}: ε_{2s}	−0.534	−0.548	−0.559
O^{2-}: ε_{2p}	−0.006	−0.016	−0.018
Y^{2-}: ε_{ns}	−0.368	−0.394	−0.364
Y^{2-}: ε_{np}	−0.018	−0.031	−0.065
Dipolar polarizability [27] (10^{-3} nm^3) $\alpha_d(U^{4+}) = 1.44$, $\alpha_d(O^{2-}) = 1.35$			
$\alpha_d(Y^{2-})$	4.89	4.57	5.01 (I^-)
Quadrupolar polarizability [27] (10^{-5} nm^5) $\alpha_q(U^{4+}) = 3.07$, $\alpha_q(O^{2-}) = 3.69$			
$\alpha_q(Y^{2-})$	19.68	14.68	15.54 (I^-)
Shielding factor [28] $\sigma^2 = 0.89$, $\sigma^4 = 0.06$, $\sigma_6 = -0.05$			

out to be the essential part of the CF potential [20]. V_C denotes the Coulomb potential of the ligand nuclei and electrons. It has been well established that V_C differs from the point charge model (PCM) prediction essentially due to the charge penetration and inter-ionic exchange effects included in V_C [20]. V_{CR} stands for the classic point charge electrostatic potential generated by the ions from outside the cluster. Contributions of electric multipoles induced on all ions in the crystal are gathered in V_{IM}. This has been determined from the crystal electrostatic equilibrium requirement [26] using literature multipole polarizabilities of the ions [27]. The shielding effect has been introduced via shielding factors σ_k, scaling the corresponding B_{kq} [28]. The data used in the calculations are listed in table 1.

3. Evaluation of the crystal field parameters

The calculated CF parameters are presented in table 2. The 'local' contribution, $V_R + V_C$, of two ligand groups, $4O^{2-}$ and $5Y^{2-}$ (sum of contributions of the two Y groups: Y_1 and Y_2) as well as the 'lattice' contribution carried by $V_{CR} + V_{IM}$ are specified there.

From the chemical context, one may expect some kind of regularity of the results along the series. However, looking at the total values of B_{kq} in table 2 only a decrease in the absolute

Table 2. Crystal field parameters (meV) calculated for UOY. The individual contribution group of ligands ($4O^{2-}$ and $5Y^{2-}$) as well as that of further neighbours and electric multipoles induced on all ions ('lattice') is specified. The shielded PCM values are given in parentheses.

		B_{20}	B_{40}	B_{44}	B_{60}	B_{64}
UOS	$4O^{2-}$	−26.8	−516.0	324.2	109.9	189.4
		(−8.6)	(−427.9)	(268.9)	(98.1)	(169.1)
	$5S^{2-}$	−82.1	165.1	−346.2	308.4	−75.8
		(−20.4)	(71.0)	(−149.4)	(43.3)	(−10.9)
	Lattice	−71.4	−193.7	−97.3	5.6	−9.2
		(38.9)	(30.4)	(−53.1)	(19.7)	(22.7)
	$\sum$	−180.4	−544.5	−119.4	423.9	104.4
		(9.9)	(−326.5)	(66.4)	(161.2)	(180.8)
UOSe	$4O^{2-}$	−50.8	−497.9	329.8	117.9	188.3
		(−16.8)	(−401.5)	(265.9)	(99.1)	(158.3)
	$5Se^{2-}$	−42.7	65.5	−311.8	337.7	−135.0
		(−4.3)	(28.7)	(−114.2)	(37.6)	(−15.0)
	Lattice	−23.6	−24.5	−108.1	0.9	23.6
		(40.8)	(27.0)	(−48.5)	(16.0)	(20.8)
	$\sum$	−117.1	−457.0	−90.1	456.5	76.9
		(19.7)	(−345.8)	(103.2)	(152.7)	(164.1)
UOTe	$4O^{2-}$	−114.0	−476.0	367.3	140.2	187.6
		(−38.4)	(−358.7)	(276.8)	(107.9)	(144.4)
	$5Te^{2-}$	−55.0	−76.7	−260.9	266.5	−161.3
		(2.7)	(−16.1)	(−78.1)	(23.3)	(−14.8)
	Lattice	10.2	−51.8	−141.0	6.6	44.8
		(52.2)	(33.1)	(−38.3)	(10.9)	(19.5)
	$\sum$	−158.8	−604.6	−34.6	413.3	71.0
		(16.4)	(−341.7)	(160.3)	(142.2)	(149.1)

values of the contribution from the chalcogenide group $5Y^{2-}$ can be noticed. This becomes more apparent in figure 1, which displays the CF strength parameter defined as a weighted square average of B_{kq}

$$N_\nu = \left[\frac{4\pi}{2k+1}\sum_{k,q}|B_{kq}|^2\right]^{1/2}. \tag{3}$$

In parallel, the absolute value of the contribution of the oxygen group, $4O^{2-}$, to N_ν is increased slightly despite a corresponding moderate decrease observed for the individual parameters B_{40} and B_{64}.

Note in table 2 the relatively small total values of the tetragonal parameters B_{k4} ($k = 4, 6$) being a consequence of opposite contributions of the oxygen and chalcogenide groups. This is in conflict with some previous findings, where the CF potential has been thought to be the cubic one perturbed with the $B_{20}C_{20}$ term only [6, 11–13]. In the light of the current results, it seems that the D_{4d} point symmetry might rather be an acceptable approximation. This feature is manifested increasingly on going from UOS to UOTe. It is worth noting that the calculation errors may cumulate undesirably in the case of competing contributions coming from particular groups of ligands. Therefore, the small values of the tetragonal parameters cannot be treated too rigorously.

Two axial parameters, B_{40} and B_{60}, seem to be the most important ones. Between them the B_{60} parameter does not change much on going from compound to compound. Hence, the

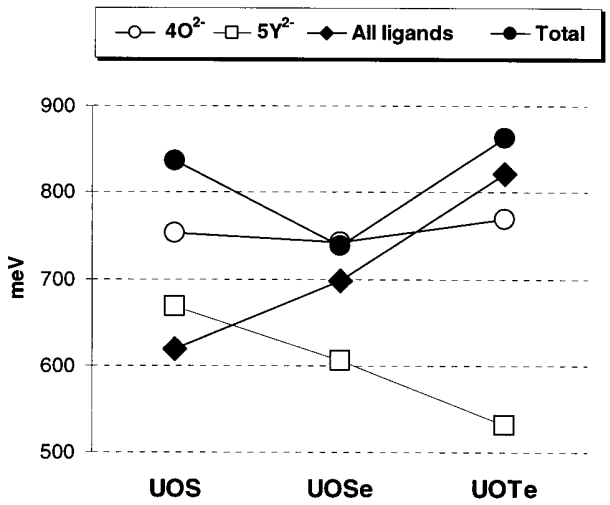

Figure 1. CF strength parameter N_v corresponding to the specified groups of ligands and total values of the CF parameters listed in table 2.

behaviour of the CF strength parameter, $N_v^{(All\ ligands)}$, attributed to ligands only, is determined mainly by B_{40}. A strong decrease in the chalcogenide contribution to this parameter inverts a weak upward tendency observed for the negative and dominating oxygen contribution. Consequently, the combined effect of the two groups of ligands, measured by $N_v^{(All\ ligands)}$, is clearly increased, just against expectations. Inclusion of both the further neighbour contribution and the polarization effects (i.e. the 'lattice' contribution $V_{CR} + V_{IM}$) destroys this inverted order. As the result, the total CF strength parameter N_v turns out to be almost the same for UOS and UOTe and only somewhat weaker for UOSe.

Generally, an interplay of contributions of various ligand groups in UOY leads to total values of the CF parameters that cannot be traced on the basis of simpler approaches than that used here. This seems to be a natural feature of the systems with two or more chemically non-equivalent ligands. It is well known that the point charge model applied to an equivalent-ligands system gives second-order CF parameters that are highly overestimated, the sixth-order parameters underestimated and fourth-order parameters within an error of, say, 50% of their actual values. It stands to reason that no such rules can be observed in compounds with non-equivalent ligands like UOY (see the PCM values given in parentheses in table 2): the O^{2-} and Y^{2-} ions are indistinguishable in the frame of PCM.

4. Simplified phenomenological approach

As mentioned in the introduction, there exist several examples indicating that the simple perturbation model here employed provides reliable estimation of the CF effect in actinide compounds. Nevertheless, it is understandable that the accuracy of such a prediction is limited and any refined analysis of the experimental data needs tools that are more precise. The uncertainty concerns not only the aforementioned problem of adequacy of the model constructed for purely ionic crystals but also some inherent approximations discussed earlier [19, 23]. The additional error caused by the presence of non-equivalent groups of ligands, as discussed above, increases this scepticism.

On the other hand, there are too many CF parameters in comparison with the available experimental data for UOY to adjust them in the conventional phenomenological approach reliably. The natural solution is to find such a simplified phenomenological model that takes advantage of the obtained theoretical results.

A natural concept and one of the most efficient is based on a partitioning of the neighbourhood of a metal ion into certain specified non-overlapping cells, while preserving the metal site symmetry [23]. Consequently, the CF potential V is assumed to have the form of a superposition of the cell potentials v^t:

$$V = \sum_t v^t. \tag{4}$$

Then, by using the rotation operators, the matrix elements of V can be expressed in terms of the matrix elements of the single cell potentials v^t, evaluated in the most convenient local coordinate system.

Such a cellular partitioning has a formal character and there is no loss in generality up to here. The main approximation refers to the local symmetry of the cells. Namely, it is assumed to be axial. Numerical simulations, performed for several actinide systems, seem to justify this assumption [29]. To facilitate further approximations, it is common to assume that each cell contains a single ligand and that the cell potential v^t can be approximated satisfactorily by an effective potential generated by this ligand.

4.1. Approaches based on the cellular decomposition

Several various parametrization schemes based on the cellular decomposition can be found in the literature. In principle they resolve themselves into two the most common ones: the angular overlap model (AOM, see [23] [29] and references therein) and the Newman superposition model (SM) [25].

The AOM parameters represent the matrix elements of potential v^t determined in the coordinate system t in which v^t is diagonal,

$$e^t_\mu = \langle 5\mathrm{f}\mu|v^t|5\mathrm{f}\mu\rangle_t \tag{5}$$

where $\mu = 0(\sigma), \pm1(\pi), \pm2(\delta)$ denotes the magnetic quantum number of the 5f electron in this coordinate system. Conventionally, the e_μ parameter with $\mu = \pm3$ is set to zero which is nothing more than a specific choice of the beginning of the energy scale.

In turn, the SM parameters b^t_k are defined by the expansion of v^t into the spherical harmonics, in a similar manner as in (1) but in the coordinate system of ligand t:

$$v^t = \sum_k b^t_k C^t_{k0}. \tag{6}$$

Due to the assumed axial symmetry, the expansion (6) contains only terms with $q = 0$, $b_k \equiv b_{k0}$. Since the e^t_μ and b^t_k parameters describe a separated ML system (linear ligator), they are called 'intrinsic parameters' as opposed to the global parameters B_{kq}.

From the above definitions (5), (6) and properties of spherical harmonics, one can easily obtain the following relation between the SM and AOM parameters:

$$\begin{aligned} 14b_2 &= 10e_\sigma + 15e_\pi \\ 7b_4 &= 9e_\sigma + 3e_\pi - 21e_\delta \\ 70b_6 &= 130e_\sigma - 195e_\pi + 78e_\delta. \end{aligned} \tag{7}$$

It is seen that, as long as a single ligand contribution is considered, the two approaches AOM and SM are algebraically equivalent. Advantages of the parametrizations based on

Table 3. AOM parameters (meV) corresponding to the 'local' contributions to the CF potential. The U^{4+}–Y^{2-} average parameters are defined by the expression $e_\mu \equiv (4e_\mu^{Y(1)} + e_\mu^{Y(2)})/5$. The ligand averaged parameters are defined by $e_\mu \equiv (4e_\mu^0 + 4e_\mu^{Y(1)} + e_\mu^{Y(2)})/9$.

	e_σ	e_π	e_δ
UOS			
U^{4+}–O^{2-}	340.1	210.5	62.8
U^{4+}–S^{2-} (1)	214.7	98.3	33.0
U^{4+}–S^{2-} (2)	194.5	86.6	28.6
U^{4+}–S^{2-} average	210.7	95.9	32.1
Ligand average	268.2	146.9	45.8
UOSe			
U^{4+}–O^{2-}	324.1	196.5	55.2
U^{4+}–Se^{2-} (1)	211.0	94.6	32.2
U^{4+}–Se^{2-} (2)	174.8	77.3	26.5
U^{4+}–Se^{2-} average	203.8	91.1	31.1
Ligand average	257.3	137.9	41.8
UOTe			
U^{4+}–O^{2-}	316.3	185.8	46.4
U^{4+}–Te^{2-} (1)	204.2	100.6	34.7
U^{4+}–Te^{2-} (2)	106.4	47.8	17.2
U^{4+}–Te^{2-} average	184.7	90.0	31.2
Ligand average	243.2	132.6	37.9

the idea of cellular partitioning are not apparent for the considered systems containing non-equivalent groups of ligands. Instead of five usual CF parameters, one obtains as many as nine intrinsic parameters, which describe the three groups of ligands. The strength of this approach, however, stems from the fact that the local ML interaction is specific for a given pair of ions and it is subject to some general rules. These rules allow one to verify phenomenological results on the one hand and indicate successive approximations on the other. The latter can be deduced either from phenomenological data available in the literature or, in the case of a lack of such data, from *ab initio* calculations. Since the AOM parameters seem to have clearer physico-chemical meaning [29], mainly this approach will be considered hereafter.

The theoretical values of the AOM parameters attributed to the 'local' components, $V_R + V_C$, of the CF potential (2) are shown in table 3. It is seen that they reflect clearly the spectrochemical ordering of the anions—the feature not being observed with the usual CF parameters. Moreover, they are ordered as follows: $e_\sigma^t > e_\pi^t > |e_\delta^t|$. The e_σ^t and e_π^t parameters depend essentially on the dominating renormalization terms included in V_R. Therefore, they can be easily estimated from squares of ML overlap integrals. Since the parameters are characteristic of given ML system, the ratios $e_\mu^t/e_\mu^{t'}$ for any two ML pairs and the ratios $e_\mu^t/e_{\mu'}^t$ in various compounds should be approximately constant. The relatively small values of e_δ suggest that this parameter can be ignored in initial steps of AOM fitting of experimental data. However, just this parameter has been shown to be 'lattice sensitive' [29], i.e. its actual value estimated from the total CF parameters is not characteristic of a given ML pair—it depends essentially on the 'lattice' contribution $V_{CR} + V_{IM}$. Therefore, it should be treated with special care.

The relations between the usual CF parameters and the AOM parameters are given in the appendix. They may be useful in initial interpretation of the experimental data (see the example considered in section 6). They also allow one to establish probable limits of the actual values of the B_{kq} parameters by a restricted variation of the e_μ^t parameters around their

theoretical values. Note how the interplay of the values of the intrinsic parameters e^t_μ and the geometrical coefficients in equations (A2)–(A4) is reflected in the discussion of the CF parameters in section 3.

In principle, the six AOM parameters in relations (A2)–(A4) must be dependent, hence, these relations cannot be applied directly. In order to reduce the number of intrinsic parameters, further simplifications are necessary. Possible steps in this direction need to be carefully verified in each individual case. Apart from omitting the e_δ parameters suggested above, one can fix either the $e^t_\mu/e^t_{\mu'}$ ratios for a given ML system t or the e^Y_μ/e^O_μ ratios. Naturally, any combination of these approximations is possible as well. The results of the *ab initio* calculations collected in table 3 provide a good basis for this kind of speculation.

4.2. Dependence of the intrinsic parameters on ML distance

The chalcogenide anions in the coordination polyhedron occur at two different distances from the uranium ion. The averaged parameters describing both chalcogenide groups have been defined by taking the theoretical ratios between the intrinsic parameters, $e^Y_\mu/e^{Y'}_\mu$. In general, a dependence of the intrinsic parameters e_μ and b_k on ML distance R can be treated as an additional characteristic of a given ML pair. The functions $e_\mu(R)$ and $b_k(R)$ are useful not only in reduction of the number of independent parameters in the case of non-equivalent ligands. They are also invaluable in investigation of the properties of solids under pressure, structural phase transitions, electron–phonon couplings and so on. Now we can derive these functions from the model calculations.

The simulations of the $e_\mu(R)$ and $b_k(R)$ functions have been performed for all the linear ligators occurring in the UOY series: U^{4+}–O^{2-}, U^{4+}–S^{2-}, U^{4+}–Se^{2-} and U^{4+}–Te^{2-}. The ML distances were varied from 0.21 nm to 0.35 nm with a step of 0.01 nm. To ensure the most reliable environment of the ions and comparability of the results obtained for the different ML pairs, a virtual ML_2 crystal of the CaF_2-type structure has been constructed for each of them. Ligands form a cubic coordination there. A variation of the ML distance R corresponds to a variation of the lattice parameter 'a': $R = 3^{1/2}a/4$.

The Madelung potential at the L and M sites in this structure is given by the formulae: $U^L = -8.141e/a$ and $U^M = 15.132e/a$, respectively. The intrinsic parameters depend on U^L and U^M in a non-trivial way through the zero-order wavefunctions and explicitly through the renormalization terms in the ligand potential v^t. Therefore, successive sets of free-ion wavefunctions for anions have been generated for each R. The radius D of the stabilizing potential wells has been assumed to be given by the expression: $D = -2e/U^L$.

The results are shown in figure 2. According to the expectations, the distance dependence of the AOM parameters has an exponential character for the ML distances being close to the real ones due to the predominating renormalization terms in this region. For larger distances, where the electrostatic contributions become important, it can be described by a power function.

As figure 2 demonstrates, the slope of the $e_\sigma(R)$ curves decreases at smaller distances on going from the oxide to telluride systems. It goes even through a maximum for the U^{4+}–Te^{2-} system. This effect is also reflected in the b_k parameters. It is interesting to note that b_6 and, to a lesser extent, b_4 becomes negative for small distances, which is characteristic of metallic systems [30]. It has been argued that several mechanisms might be responsible for that: virtual bond state, hybridization between 5f and conduction electron wavefunctions or anti-shielding effects [31]. From the present simulations, it is clear that also mechanisms characteristic of ionic systems may lead to the negative values of the intrinsic parameters. Observation of the individual contributions, specified in equation (2), indicates a rapidly growing charge

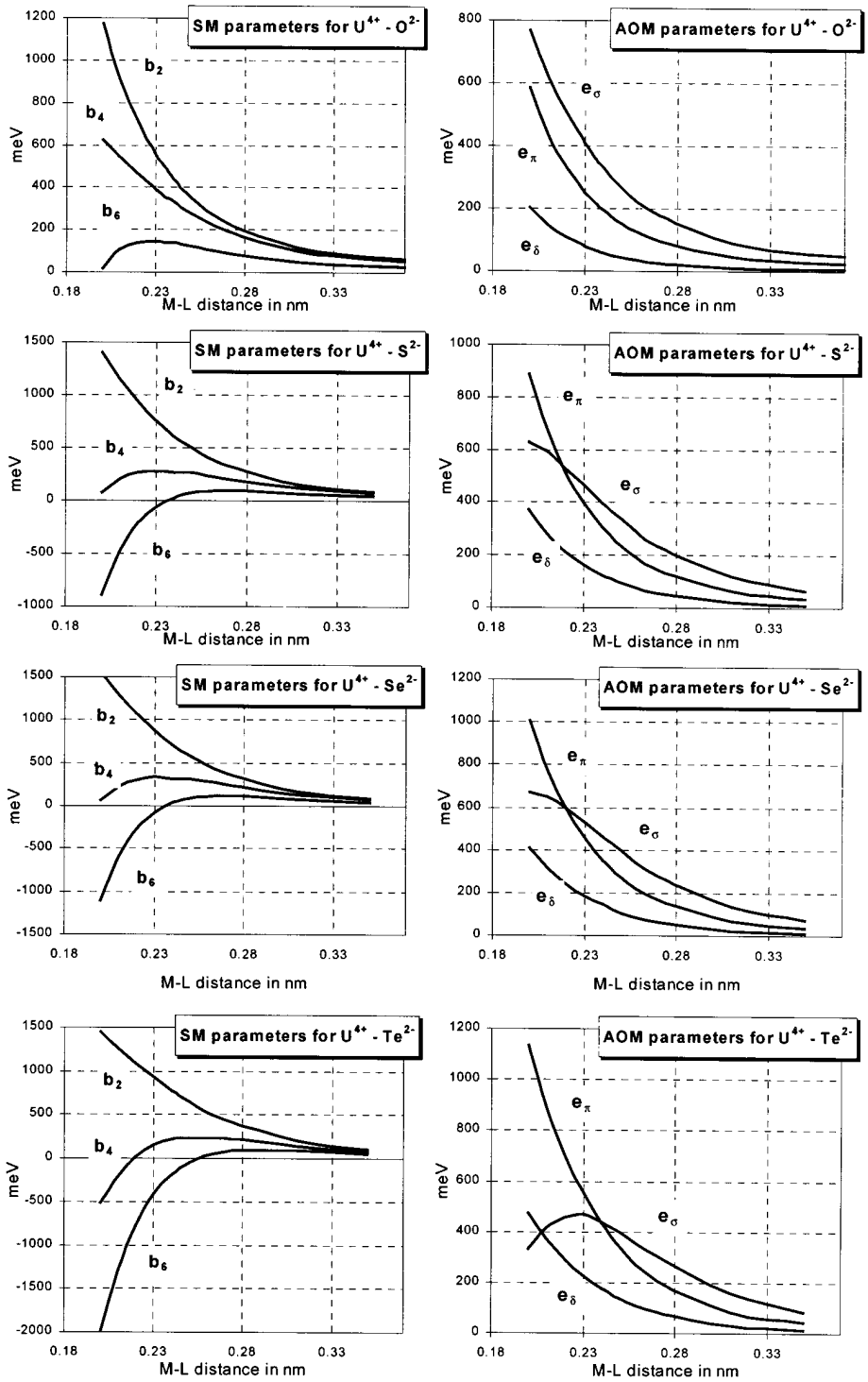

Figure 2. Dependence of SM and AOM intrinsic parameters on ML distance in a virtual crystal of the CaF_2-type structure.

Table 4. Distance dependence of the AOM parameters (in meV) approximated by the power function $e_\mu = aR^{-b}$ in the range of 0.21–0.27 nm for U^{4+}–O^{2-} and 0.25–0.35 nm for U^{4+}–Y^{2-}.

	a	*b*
U^{4+}–O^{2-}		
e_σ	0.305 55	4.887
e_π	0.033 21	6.076
e_δ	0.002 65	7.005
U^{4+}–S^{2-}		
e_σ	0.398 51	4.869
e_π	0.052 83	6.062
e_δ	0.005 84	6.971
U^{4+}–Se^{2-}		
e_σ	0.400 41	4.983
e_π	0.047 21	6.251
e_δ	0.005 91	7.074
U^{4+}–Te^{2-}		
e_σ	0.940 70	4.379
$e\pi$	0.053 11	6.324
e_δ	0.009 93	6.892

penetration and metal–ligand exchange with respect to the other mechanisms. Relatively small interionic distances occurring for metallic systems promote such behaviour.

For practical purposes, the $e_\mu(R)$ dependences have been approximated by simple power functions. This can always be done in the case of small enough distance intervals. The obtained multiplicative coefficients and the exponents are listed in table 4. The exponents are lower than those estimated before [29]. For instance, the previous values of 6.71, 7.59 and 7.10, reported for the U^{4+}–O^{2-} system, now amount to 4.89, 6.08 and 7.01 for the e_σ, e_π and e_δ parameters, respectively. The difference is a consequence of the fact that the same set of free-ion wavefunctions has previously been used for each ML distance independently on the actual Madelung potential. Now, the free-ion orbitals are generated with the Madelung-like potential varying with the distance according to the above expressions. A similar reduction of the power exponents for the same reason has recently been reported for the Pr^{3+}–Cl^- system [32].

5. Ground state properties

The electronic structure of a bound ion is determined with the following phenomenological Hamiltonian, defined in the convenient function basis span by the Russell–Saunders ${}^{2S+1}L_{J,M}$ states:

$$H = H_0 + V \tag{8}$$

where the non-spherical part V has the form of equation (1) and the spherical ('free-ion') part can be written as:

$$H_0 = \sum_k F^k \boldsymbol{f}_k + \sum_i \zeta_i \boldsymbol{l}_i \cdot \boldsymbol{s}_i + H^{CI}. \tag{9}$$

According to the conventional notation, $\boldsymbol{f}_k$ and $\boldsymbol{l}_i \cdot \boldsymbol{s}_i$ represent an angular part of interelectron repulsion and spin–orbit interaction, respectively. F^k and ζ_i are the corresponding radial integrals. For the present purpose, the values of $F^2 = 5339$ meV, $F^4 = 4833$ meV,

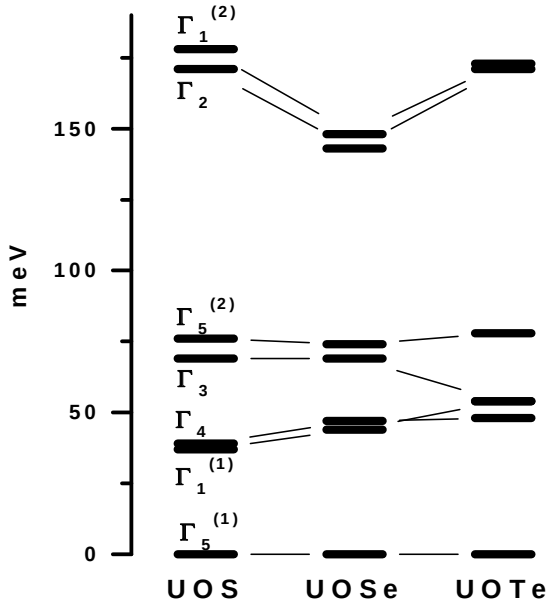

Figure 3. The lowest part of the energy spectrum obtained by diagonalization of Hamiltonian (8) with the CF parameters determined from the *ab initio* calculations (table 2).

$F^6 = 3024$ meV and $\zeta = 224$ meV, reported for U^{4+} in $ThGeO_4$ [33] have been accepted. The corrections of higher order due to the configuration interaction and relativistic effects gathered in H^{CI} are to ensure that the free-ion electronic structure is adequately represented. Simultaneous diagonalization of all terms in the Hamiltonian (8), (9) leads to mixed states in a form of linear combinations of the $^{2S+1}L_{J,M}$ functions, characterized by the irreducible representations of the C_{4v} point group: four singlets—Γ_1, Γ_2, Γ_3, Γ_4—and one doublet–Γ_5.

The low energy levels obtained with the above free-ion parameters and with the CF parameters from table 2 are shown in table 5 and in figure 3. As seen, the doublet $\Gamma_5^{(1)}$ is the ground state for each member of the series. The excited levels are arranged into three groups: around 40–50 meV ($\Gamma_1^{(1)}$, Γ_4), 70–80 meV (Γ_3, $\Gamma_5^{(2)}$) and 150–170 meV ($\Gamma_1^{(2)}$, Γ_2), except for Γ_3 of UOTe, which is moved from the second to the first group. The composition of the wave-vectors shown in table 5 indicates that the effect of term mixing depends quantitatively as well as qualitatively on the transformation symmetry of state. The largest mixing takes place for the Γ_4 state and the smallest for Γ_5. The contribution of the components originating from the $^3H_4$ term varies from 0.84 to 0.90, respectively.

Magnetic and thermodynamic properties are determined essentially by the ground state and the first two groups of excited states listed in table 5. The third group may be considered as located beyond the temperature range of interest. Examples of temperature dependences of the van Vleck magnetic susceptibility, Schottky heat capacity and entropy, in the paramagnetic range are presented in figure 4. They have been obtained using the standard formulae describing these quantities. The matrix elements for the Zeeman operator in the van Vleck formula have been evaluated using all components of the mixed states included in the calculations. For the sake of clarity, any corrections for the ordered phase have not been included. Nevertheless, at temperatures sufficiently above the critical point, these corrections lead only to a displacement of the reciprocal susceptibility and do not influence its shape. The same holds for the entropy plot. The displacements are determined by the parameters characterizing the ordering

Table 5. The energy (in meV) and composition of the lowest eigenstates of dominating $^3H_4$ components in the $^{2S+1}L_{J,M}$ function basis.

State	Energy	Main components
UOS		
$\Gamma_5^{(1)}$	0.0	$-0.9036\,^3H_{4,-3} - 0.2796\,^1G_{4,-3} + 0.2723\,^3H_{4,1}$
$\Gamma_1^{(1)}$	37.0	$0.9006\,^3H_{4,0} - 0.2552\,^3F_{2,0} + 0.2392\,^1G_{4,0} - 0.1563\,^3H_{4,4} - 0.1563\,^3H_{4,-4}$
Γ_4	39.4	$-0.6498\,^3H_{4,-2} + 0.6498\,3H_{4,2} - 0.2519\,^1G_{4,-2} + 0.2519\,^1G_{4,2} + 0.1075\,^3F_{4,-2} - 0.1075\,^3F_{4,2}$
Γ_3	68.9	$0.6578\,^3H_{4,2} + 0.6578\,^3H_{4,-2} + 0.2342\,^1G_{4,2} + 0.2342\,^1G_{4,-2}$
$\Gamma_5^{(2)}$	76.0	$0.8956\,^3H_{4,1} + 0.2881\,^3H_{4,-3} + 0.2797\,^1G_{4,1} - 0.1045\,^3F_{3,1}$
UOSe		
$\Gamma_5^{(1)}$	0.0	$0.9266\,^3H_{4,-3} + 0.2819\,^1G_{4,-3} - 0.1988\,^3H_{4,1}$
$\Gamma_1^{(1)}$	44.3	$-0.9111\,^3H_{4,0} - 0.2435\,^1G_{4,0} + 0.2196\,^3F_{2,0} + 0.1559\,^3H_{4,4} + 0.1559\,^3H_{4,-4}$
Γ_4	47.1	$0.6500\,^3H_{4,-2} - 0.6500\,^3H_{4,2} + 0.2518\,^1G_{4,-2} - 0.2518\,^1G_{4,2} - 0.1074\,^3F_{4,-2} + 0.1074\,^3F_{4,2}$
Γ_3	68.9	$0.6557\,^3H_{4,2} + 0.6557\,^3H_{4,-2} + 0.2385\,^1G_{4,2} + 0.2385\,^1G_{4,-2}$
$\Gamma_5^{(2)}$	73.7	$-0.9172\,^3H_{4,1} - 0.2895\,^1G_{4,1} - 0.2096\,^3H_{4,-3} + 0.1075\,^3F_{3,1}$
UOTe		
$\Gamma_5^{(1)}$	0.0	$0.9439\,^3H_{4,-3} + 0.2945\,^1G_{4,-3}$
Γ_4	47.6	$0.6502\,^3H_{4,2} - 0.6502\,^3H_{4,-2} + 0.2475\,^1G_{4,2} - 0.2475\,^1G_{4,-2} - 0.1032\,^3F_{4,2} + 0.1032\,^3F_{4,-2}$
$\Gamma_1^{(1)}$	53.8	$-0.9209\,^3H_{4,0} + 0.2548\,^3F_{2,0} - 0.2487\,^1G_{4,0}$
Γ_3	54.2	$-0.6554\,^3H_{4,-2} - 0.6554\,^3H_{4,2} - 0.2381\,^1G_{4,-2} - 0.2381\,^1G_{4,2}$
$\Gamma_5^{(2)}$	78.3	$-0.9330\,^3H_{4,1} - 0.2935\,^1G_{4,1} + 0.1188\,^3F_{3,1}$

interaction and can be discussed independently. A fluctuation tail of the lambda-shape anomaly in the heat capacity is practically negligible in this range of temperatures.

The longitudinal susceptibility depends efficiently on the ground state doublet. The theoretical values of its magnetic moment, 2.048, 2.191 and 2.345 μ_B, can be compared with the experimental ones of 2.0, 2.2 and 2.0 μ_B determined for UOS, UOSe and UOTe, respectively [10]. We observe a quite good agreement except for UOTe. Note that, in the case of purely axial CF field, the ordered moment of uranium reaches as high as a value of $3\,\mu_B$. An admixture of the $|\pm 1\rangle$ component to the $|\pm 3\rangle$ state by the tetragonal terms $B_{k4}C_{k4}(k = 4, 6)$ of the CF potential lowers the magnitude of the moment. Thus, the lower the values of the $|B_{k4}|$, the higher the magnitude of the moment.

The transverse susceptibility and the remaining thermodynamic quantities are sensitive to details of the intrinsic structure of the first two groups of excited levels. As seen from figure 4, there are no striking differences between the compounds in the simulated temperature characteristics. The increase in magnetic moment along the series mentioned above is accompanied by an advancing concave character of the reciprocal longitudinal susceptibility in the 100–400 K interval. Simultaneously, weakening of the transverse susceptibility and somewhat slower increase in the entropy as a function of temperature is revealed. Surprisingly, the maximum of the Schottky heat capacity for UOTe occurs between such maxima as observed for UOS and UOSe.

The above numerical simulations have been performed in order to compare the theoretical results along the series in terms of the measurable quantities. They may also play a role of reference data in discussion of actual properties of the compounds under consideration. Nevertheless, their thorough analysis needs further extensive works that go beyond the scope of this report. It is only worth noting that the current results are consistent with some findings reported hitherto. This concerns, for example, the recent analysis of magnetic properties in

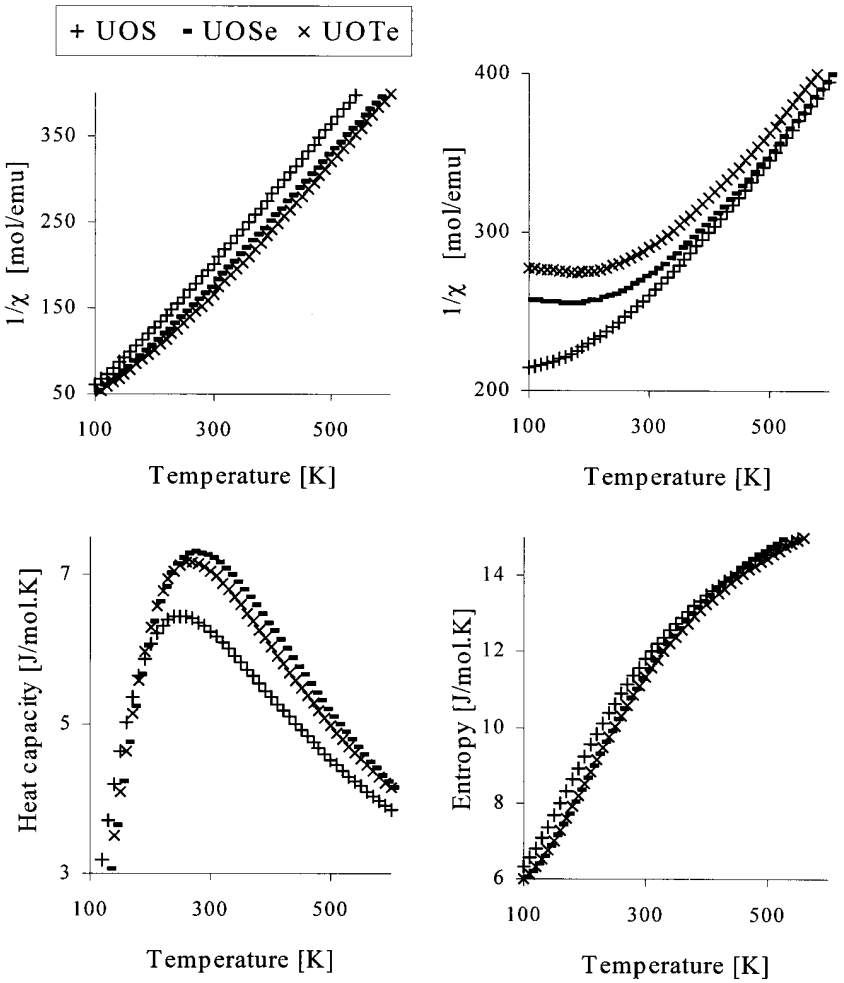

Figure 4. Model temperature dependences of parallel and perpendicular reciprocal magnetic susceptibility, Schottky heat capacity and entropy.

UOSe [7]. However, there also exists an uneasy interpretation of the electronic structure of UOS [11], which is not convergent with our results. The latter problem will be addressed in the next two sections. Both recognition of the experimental situation and its understanding are less advanced in the case of UOTe. New structural and magnetic investigations for UOTe are now in progress [34]. This may make the discussion of its electronic properties more comprehensive in the future.

6. Application to the INS spectra of UOS

The INS spectra of UOS have initially been discussed in a series of papers by Amoretti *et al* [11, 13, 24] in which the experimental data have also been reported. Several different CF splitting schemes of the ground $^3H_4$ term have been considered there. The authors

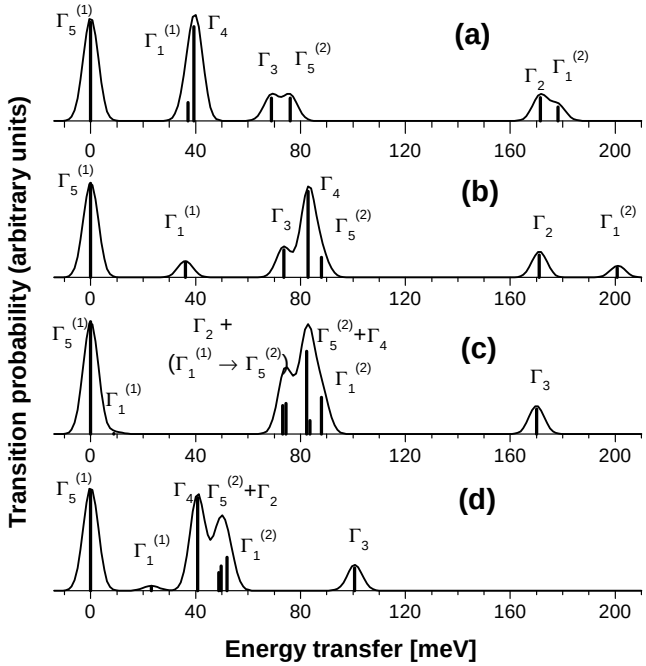

Figure 5. Magnetic transitions simulated for UOS in different approaches: (a) *ab initio* calculations, (b) using the CF parameters adjusted to the observed INS transitions [11] according to model II described in the text, (c) model (iii) by Amoretti *et al* [11], (d) using the same set of the CF parameters as in (c) but taking into account the mixing of terms.

Table 6. Comparison of the various sets of CF parameters (meV) for UOS.

	B_{20}	B_{40}	B_{44}	B_{60}	B_{64}
Amoretti *et al* [11]	31.4	−80.2	−127.6	595.5	−243.0
Ab initio calculations	−180.4	−544.5	−119.4	423.9	104.4
Model I	−116.6	−566.7	−10.6	632.3	250.0
Model II	−146.5	−579.4	−38.8	595.1	447.1

have followed various electrostatic models known from their earlier works on spectroscopic and magnetic properties of other uranium compounds. In the latest interpretation of the UOS electronic structure (model (iii) of [11]) they have fitted the CF parameters directly to the observed INS transition energies and intensities, starting with one of the energy level assignments supported by the electrostatic models considered earlier. The fitting was very precise in the experimentally most pronounced region 60–100 meV. For the present purpose it has been restored in the form of the model INS spectrum shown in figure 5(c) (see the comment below). In obtaining this figure we have followed the original calculations, which have been carried out in the function basis reduced to the pure Russell–Saunders $^3H_{4,M}$ states with the CF parameters quoted in table 6. Further on in this report, figure 5(c) is treated as representing the experimental INS lines in the above energy region. The reader interested in the actual experimental data is referred to the original papers [11, 13, 24].

Figure 5 displays the magnetic dipole transitions *simulated* using various CF models discussed herein, including the model proposed by Amoretti *et al*, mentioned above.

The simulations are not referred in this figure directly to the experimental recordings. Therefore, neither the Debye–Waller factor nor the 5f-electron form factor is taken into account since these quantities do not depend on the distribution of levels or their compositions. We concentrate on the transition probabilities, which depend on matrix elements of the Zeeman operator [35]. Thus, the value of each data point, represented as the height of a column in figure 5, is proportional to the sum of squares of the matrix elements of the Zeeman operator components between the initial Γ_i and final Γ_j states,

$$Z_{ij} = \frac{2}{3} \sum_{\nu_i, \nu_j} \sum_{\alpha = x,y,z} \langle \Gamma_i, \nu_i | \boldsymbol{L}_\alpha + 2\boldsymbol{S}_\alpha | \Gamma_j, \nu_j \rangle \tag{10}$$

where ν_i, ν_j identifies individual components of the eigenvectors in the case of the degenerate states.

The line graphs represent the same data in the form of the Gaussian distributions of arbitrarily chosen half width of $\sim$4 meV. They have only an illustrative character.

Despite high accuracy in matching the INS transition energies and their relative intensities, the interpretation (iii) given by Amoretti *et al* [11] raises some doubts. Firstly, the values of B_{20}, B_{40}, B_{64} are considerably different than those resulting from the *ab initio* calculations (see table 6). Secondly, application of the pure Russell–Saunders coupling, as has been done in [11], may cause some deformations of the results. More precisely, the relatively strong CF and spin–orbit interactions, characteristic of the bonded uranium (4+) ion in a typical crystal, should incline one to check to what extent the effect of the term mixing influences the results. This can easily be done by simultaneous diagonalization of all the interactions included in Hamiltonian (8) with the original set of CF parameters, allowing for the extended function basis spanned by all the $^{2S+1}L_{J,M}$ states of the electron configuration $5f^2$. The result is shown in figure 5(d). Usually, some moderate modifications of the energies of levels and the corresponding wavefunctions are expected. Surprisingly, figure 5(d) looks entirely different from figure 5(c). Thus, it seems that the interpretation of the CF effect given in [11] and consequently the CF parameters there reported may be not quite reliable.

An alternative interpretation of the INS spectra can be developed starting with the results of the *ab initio* calculations. It has already been noticed that the energy levels obtained with the theoretical CF parameters are grouped at around 40 and 70 meV. This looks quite promising in light of the observed energies of the INS transitions. A slight modification of the CF parameters adjusts the $\Gamma_5^{(1)} \rightarrow \Gamma_3$ and $\Gamma_5^{(1)} \rightarrow \Gamma_5^{(2)}$ intervals to the experimental ones: 74 and 83 meV. A problem arises, however, when we tray to calculate intensities of these transitions: the above two lines have turned out to be too weak in comparison with those of the lower part of the calculated spectrum determined by the $\Gamma_5^{(1)} \rightarrow \Gamma_1^{(1)}$ and $\Gamma_5^{(1)} \rightarrow \Gamma_4$ excitations. This is shown in figure 5(a). Comparison with plot (c), representing the experimental data, suggests another assignment of the energy levels. Namely, it seems probable that the most intense transition $\Gamma_5^{(1)} \rightarrow \Gamma_4$ located at 39 meV in plot (a) should correspond to the experimental line observed at 83 meV. Consequently, the structures observed at 74 and 87 meV can be assigned to the $\Gamma_5^{(1)} \rightarrow \Gamma_3$ and $\Gamma_5^{(1)} \rightarrow \Gamma_5^{(2)}$ transitions, respectively. It has been verified that several other possible assignments lead to unsatisfactory results.

The present task is to adjust as many as five CF parameters to only four measured quantities: three INS transition energies and the value of the ordered magnetic moment ($2\,\mu_B$). In addition, the solution of the fitting procedure should preserve at least approximately the experimental relative intensities of the transitions. The problem becomes tractable with aid of the angular overlap model (AOM) discussed in section 4. The relations between the B_{kq} parameters and the average AOM parameters e_μ ($\mu = \sigma, \pi, \delta$) adopted for the present needs are given in equations (A5) in the appendix.

Thus, the initial fitting (model I) has been performed using a standard simultaneous diagonalization routine adapted for the AOM parametrization according to the equations (A5). As a result, the assigned energies have been matched exactly the observed values but not the magnitude of the ordered moment. The obtained AOM parameters (in meV), $e_\sigma = 314.9$, $e_\pi = 137.7$, $e_\delta = 15.9$, are relatively close to the *ab initio* values determined on the basis of the 'local' only contributions, which amount to 268.2, 146.9, 45.8 meV, respectively. The corresponding B_{kq} parameters, presented as 'model I' in table 6, are close to the theoretical values except for the tetragonal ones B_{k4}, $k = 4, 6$. However, just these parameters have been demonstrated in section 3 to be inherently less reliable when evaluated from first principles.

The results obtained within model I may serve now as initial data in a more precise fitting in which the AOM constraints are released. Both the relative intensities of the transitions and the value of the ground state moment ($\mu = 2\ \mu_B$) can readily be matched by a further adjustment of the ordinary CF parameters B_{kq}. Nonetheless, there still exists infinity of solutions fulfilling all these requirements. It has been checked that for any value of the B_{20} parameter, varied within the range from -50 to -223 meV, an acceptable solution can be found by adjusting the remaining parameters. The position of the first excited level, $\Gamma_1^{(1)}$, has turned out to be almost fixed in these simulations. Simultaneously, the positions of the Γ_2 and $\Gamma_1^{(2)}$ levels have increased from 123 to 211 meV and (from 171 to 231 meV, respectively) and so has the overall splitting of the $^3H_4$ term.

The revealed indefiniteness of the latest fittings is a problem, which cannot be resolved to the end without supplementary experimental data. Nevertheless, we can indicate a solution imposing two additional contradictory requirements. On the one hand, it seems natural to assume that the overall CF splitting of the $^3H_4$ term is as close to that inferred in model I as possible. On the other, it should be taken into account that, although the experimental recordings have been extended up to energy transfers of 200 meV, no transitions have been observed above 100 meV [13]. Thus, the model transitions to the two highest levels Γ_2 and $\Gamma_1^{(2)}$ should have intensity low enough to be immeasurable under the actual experimental conditions. Generally, the intensity decreases with increasing the energy transfer. Therefore, the final solution, denoted hereafter as model II, has been chosen so as to get the lowest from these two transitions, $\Gamma_5^{(1)} \rightarrow \Gamma_2$, just at the threshold value of 170 meV, justified below. The result is visualized in figure 5(b).

The intensity of INS line is proportional to Z_{ij} given in equation (10) and to the square of magnetic form factor, $f^2(Q)$, where $\boldsymbol{Q}$ is the momentum transfer in the scattering process. The magnetic form factor decreases rapidly with increasing energy transfer above 100 meV. Suppose that lower of these two levels, Γ_2, has energy of 170 meV as in the *ab initio* calculations (see figure 5(a)). We try to compare the intensity of the INS transition to this level with the most intense line $\Gamma_5^{(1)} \rightarrow \Gamma_4$ at 83 meV. The uranium (4+) form factor can be estimated assuming, after [36], $f^2(Q) \cong \exp(-0.07Q^2)$ with Q in Å^{-1}. The original INS measurements have been performed with the neutron incident energy $E_i = 290$ meV and the scattering angle $\phi = 5^\circ$ [13]. The above data combined with the kinematic constraints of a scattering process give the form factor of value of 0.76 and 0.27 for the energy transfers of 83 and 170 meV, respectively. The corresponding Z_{ij} elements are equal to 2.44 and 0.64. Hence, the ratio of the intensities amounts to $(0.76 \times 2.44)/(0.27 \times 0.64) \cong 10.8$. This means that the analysed $\Gamma_5^{(1)} \rightarrow \Gamma_2$ transition has intensity as many as ten times less than that of the main line in the spectrum (which is located at 83 meV). In other words, just due to the two considered quantities, i.e. the transition probability and the form factor, the lines corresponding to the higher energy transfers than 170 meV may become comparable with the experimental background.

The CF parameters obtained in model II are presented in table 6. They are consistent with the remaining models discussed in this paper except again for the tetragonal parameters B_{k4}. The corresponding model INS transitions, as displayed in figure 5(b), are close to the experimental ones (figure 5(c)) in the well-established region of 60–100 meV. At lower energies the model predicts the transition $\Gamma_5^{(1)} \rightarrow \Gamma_1^{(1)}$ at about 36 meV. The existence of relatively low intensity magnetic transitions below 50 meV has not been excluded [13]. Verification of the transitions foreseen at 170 meV and above needs further INS investigations with higher neutron incident energies than those used so far.

7. Magnetic susceptibility and heat capacity of UOS

The lowest eigenstates of the phenomenological Hamiltonian (8) obtained in model II are presented in table 7. These data have been used to simulate the temperature dependences of the van Vleck magnetic susceptibility, Schottky contribution to the heat capacity, ΔC_{Sch}, and entropy, ΔS_m. The matrix elements for the Zeeman operator in the van Vleck formula have been evaluated using all components of the mixed states included in the calculations, similarly as in the case of INS transition probabilities. The simulations are compared in figure 6 with those obtained by using the results of the *ab initio* calculations and model (iii) proposed by Amoretti *et al* [11]. As in section 5 we are interested in the paramagnetic region only and, for the sake of clarity, no corrections for the ordered phase have been included in these simulations.

Table 7. The energy (in meV) and composition of the lowest eigenstates of the dominating ^{3}H$_4$ component in the $^{2S+1}L_{J,M}$ function basis obtained in model II for UOS.

State	Energy	Main components
$\Gamma_5^{(1)}$	0.0	$-0.9073\,{}^3\mathrm{H}_{4,-3} - 0.2701\,{}^1\mathrm{G}_{4,-3} + 0.2230\,{}^3\mathrm{H}_{4,1} - 0.1150\,{}^3\mathrm{H}_{5,-3} - 0.1008\,{}^3\mathrm{F}_{3,1}$
$\Gamma_1^{(1)}$	36.1	$0.8667\,{}^3\mathrm{H}_{4,0} - 0.2492\,{}^3\mathrm{H}_{4,-4} - 0.2492\,{}^3\mathrm{H}_{4,4} - 0.2418\,{}^3\mathrm{F}_{2,0} + 0.2047\,{}^1\mathrm{G}_{4,0}$
Γ_3	73.6	$0.6611\,{}^3\mathrm{H}_{4,-2} + 0.6611\,{}^3\mathrm{H}_{4,2} + 0.2277\,{}^1\mathrm{G}_{4,-2} + 0.2277\,{}^1\mathrm{G}_{4,2}$
Γ_4	82.9	$0.6273\,{}^3\mathrm{H}_{4,-2} - 0.6273\,{}^3\mathrm{H}_{4,2} + 0.2810\,{}^1\mathrm{G}_{4,-2} - 0.2810\,{}^1\mathrm{G}_{4,2} - 0.1371\,{}^3\mathrm{F}_{4,-2} + 0.1371\,{}^3\mathrm{F}_{4,2}$
$\Gamma_5^{(2)}$	88.0	$0.8966\,{}^3\mathrm{H}_{4,1} + 0.2604\,{}^3\mathrm{H}_{4,-3} + 0.2797\,{}^1\mathrm{G}_{4,1} - 0.1192\,{}^3\mathrm{F}_{3,1}$
Γ_2	171.1	$0.6476\,{}^3\mathrm{H}_{4,-4} - 0.6476\,{}^3\mathrm{H}_{4,4} + 0.2177\,{}^1\mathrm{G}_{4,-4} - 0.2177\,{}^1\mathrm{G}_{4,4} - 0.1151\,{}^3\mathrm{H}_{4,-4} + 0.1151\,{}^3\mathrm{H}_{4,4}$ $-0.1418\,{}^3H_{5,0}$
$\Gamma_1^{(2)}$	200.7	$0.5997\,{}^3\mathrm{H}_{4,-4} + 0.5997\,{}^3\mathrm{H}_{4,4} + 0.3253\,{}^3\mathrm{H}_{4,0} + 0.2220\,{}^3\mathrm{G}_{4,-4} + 0.2220\,{}^3\mathrm{G}_{4,4} + 0.1427\,{}^1\mathrm{G}_{4,0}$ $-0.1076\,{}^3H_{4,-4} - 0.1076\,{}^3H_{4,4}$

The corresponding experimental curves can be found in [10–12]. The slope of the reciprocal longitudinal magnetic susceptibility evaluated in model II and the shape of its transversal component appear to be close to those determined experimentally. The agreement seems even better than that demonstrated previously [11]. This is clearly seen in figure 7 where both the present and former interpretations are compared with the average susceptibility measured for the powdered UOS sample, restored here according to the relation (in the units of emu mol^{-1}) [10]:

$$\chi_{av} = \frac{1}{3}\chi_{\parallel} + \frac{2}{3}\chi_{\perp} = \frac{1/T + 0.0076 - 0.0064\exp(-244/T)}{2 + \exp(-244/T)}. \tag{11}$$

This time, the corrections for the ordered phase have to be included in derivation of the model temperature dependences, since they are referred in figure 7 directly to the experimental curve (11). Following [11], an anisotropic exchange interaction with two different exchange shifts of the inverse susceptibility curves, namely $\lambda_{\parallel} = 10$ mol emu^{-1} and $\lambda_{\perp} = -65$ mol emu^{-1}, has been accepted.

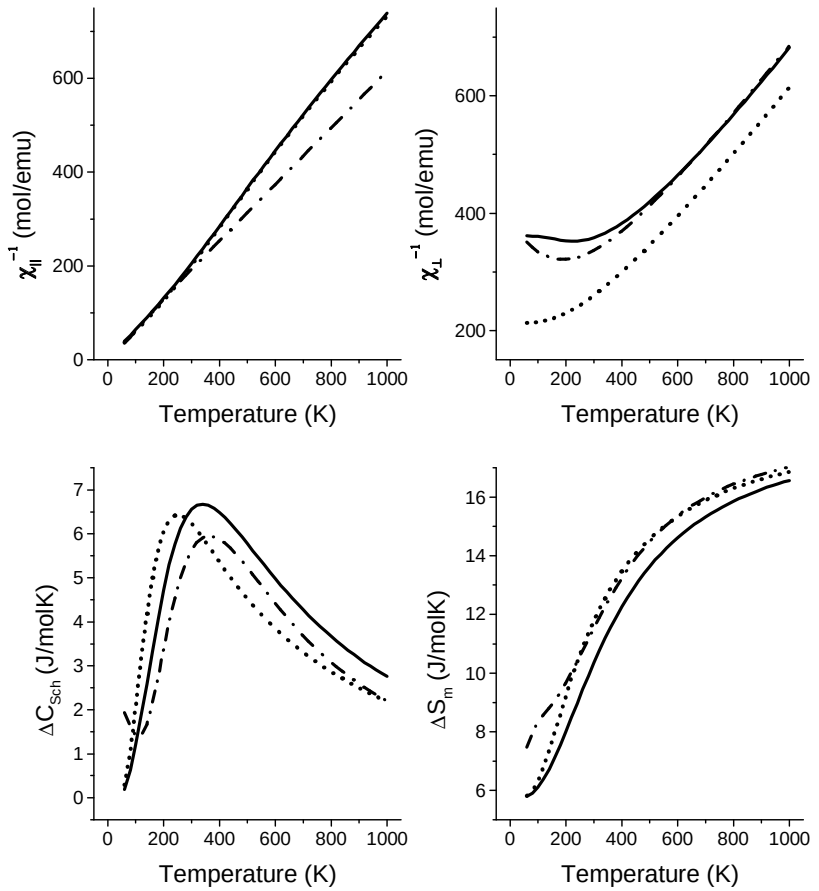

Figure 6. Comparison of longitudinal and transversal reciprocal magnetic susceptibility, Schottky contribution to heat capacity, ΔC_{Sch}, and the corresponding entropy, ΔS_m, of UOS as a function of temperature obtained in different models: model (iii) proposed in reference [11] (dash-dotted line), *ab initio* calculations (dotted line), model II of this work (solid line).

Coming back to figure 6, it is interesting to note a certain inconsistency when the model curves are referred to the experimental data. It turns out that the better the agreement of given model with the measured transversal susceptibility the larger the discrepancy in the position of the broad maximum in ΔC_{Sch}, which is observed experimentally at $T_M = 250$ K [12]. The *ab initio* model matches exactly the experimental value of T_M but it overestimates $\chi_\perp$ (especially in the temperature range of 60–300 K) whereas models II and (iii) describe satisfactorily the $\chi_\perp$ but they give T_M shifted by 90 K and 110 K, respectively. However, both the quantities depend essentially on the distribution of levels at 30–60 meV. There are two levels in this region, $\Gamma_1^{(1)}$ and Γ_4, predicted in the *ab initio* model, in contradiction to only one level ($\Gamma_1^{(1)}$) foreseen in model II or none in the case of model (iii) proposed by Amoretti *et al* [11].

It seems that these two different experiments discussed above cannot be thoroughly reconciled in the frame of a common model. The inconsistency of the magnetic and thermodynamic properties may indicate some contributions from thermal excitations to the

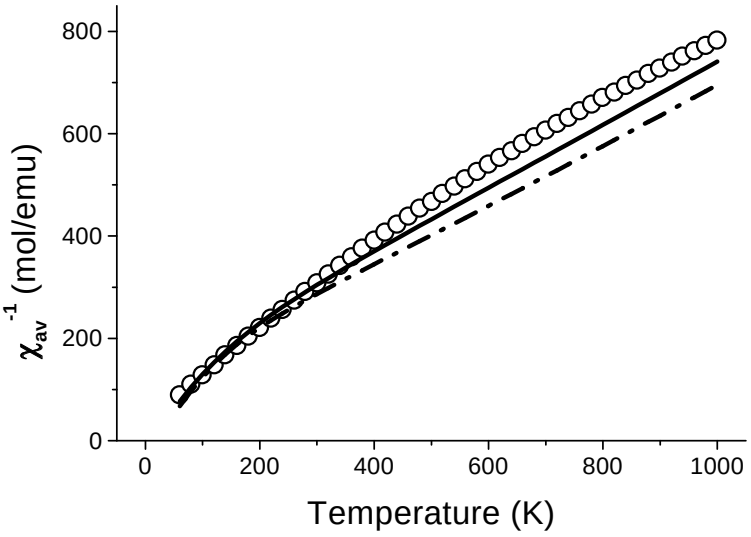

Figure 7. Temperature dependence of reciprocal magnetic susceptibility of UOS measured for polycrystalline sample [10] (open circles) in relation to the curves generated with model (iii) from [11] (dash-dotted line) and model II of the present paper (solid line).

conduction band in UOS. This is clearer if one bears in mind a relatively small gap in the electronic band structure in this compound (67.5 meV [8]) and possible impurities in the sample [8, 12]. In addition, all the model curves representing the $\Delta C_{Sch}(T)$ dependence in figure 6 are almost uniformly shifted down by 2–3 J mol^{-1} K^{-1} in relation to the experimental plot. This observation seems to confirm the suppositions concerning the ignored or hidden mechanisms that modify the thermodynamic characteristics. In general, a separation of the Schottky contribution from the measured total heat capacity can be thought to be not so rigorous and the extracted data should be treated with caution [12, 37]. However, the shape of the function may be affected to a lesser degree during such an operation. In particular, this concerns the measured position of the maximum in the $\Delta C_{Sch}(T)$ curve.

The excess magnetic entropy $\Delta S_m = 5.80$ J mol^{-1} K^{-1}, as evaluated in model II at 60 K, only slightly exceeds the ground doublet contribution, which amounts to $R \ln 2 = 5.76$ J mol^{-1} K^{-1}, and it is somewhat lower than the experimental value of 6.3 J mol^{-1} K^{-1} at 55 K deduced from the heat capacity measurements [12]. In the light of the problems with precise determination of this quantity, the prediction may be considered satisfactory, the more so as the possible mechanisms not included in the model calculations may only enlarge the entropy. This does not concern model (iii) by Amoretti *et al* [11] that foresees the $\Gamma_1^{(1)}$ level in the vicinity of the ground $\Gamma_5^{(1)}$ state. It leads to as high as ΔS_m value as 7.5 J mol^{-1} K^{-1} at 55 K, which can hardly be reconciled with the experimental value on the basis of the present understanding of the UOS properties.

8. Concluding remarks

The simple perturbation model employed in this paper seems to be a reliable tool for describing details of the electronic structure of localized states in solids. Its present application addresses the important question of systematic and consistent description of the electronic structure of

the U^{4+} ion in the series of uranium oxychalcogenides. The *ab initio* and phenomenological models here proposed can be seen as a keystone of interpretation of various experimental data for the whole series. The competition of different contributions to the CF parameters revealed with these models and their variation along the series explain apparently random total values. Nevertheless, even a rough analysis of an interplay of factors dependent on the coordination geometry and so called 'intrinsic parameters' describing the separated metal–ligand (ML) linear ligators, points to presumably rational ranges of actual values of CF parameters. In particular, the calculations evidence an axial character of the crystal field potential in exact contradiction to some earlier findings.

Dependences of the intrinsic parameters on the ML distance, R, have been examined thoroughly for the U^{4+}–O^{2-}, U^{4+}–S^{2-}, U^{4+}–Se^{2-} and U^{4+}–Te^{2-} systems. The calculation conditions have been unified to exclude host dependent effects. The anion wavefunctions have been generated for each R point according to the varying Madelung potential. The new numerical data show that these dependences are somewhat weaker than those reported before. At small ML distances, the intrinsic parameters behave in a manner characteristic of the metallic state.

Some simplifications of the common phenomenological models suggested on the basis of the *ab initio* calculations open new possibilities of interpretation of complex magnetic and other properties of UOY. The obtained eigenstates of the uranium ion and simulated temperature characteristics of such quantities as the magnetic susceptibility or heat capacity may serve as good reference data.

As an example, the theoretical results are applied to analyse the experimental data reported for UOS elsewhere. The phenomenological CF model describing the INS spectra of UOS, proposed recently by Amoretti *et al* [11], has been shown to lead to a surprisingly different energy-level scheme if the effect of the term mixing is taken into account. It has turned out to be inconsistent also with the *ab initio* calculations of the CF parameters. The alternative interpretation of the INS spectra has been developed in an extended wave-function basis, starting with the electronic level assignment deduced from the first-principles calculations. The fitting of the INS data has been performed in two steps. First, the angular overlap model has been applied to obtain the identified INS transition energies. Then, the CF parameters have been refined to obtain the measured ordered magnetic moment and the relative intensities of the INS transitions. Both the intermediate and final sets of CF parameters appear consistent with the initial *ab initio* values. A good agreement with the INS data has been achieved in the experimentally most pronounced energy region, i.e. 60–100 meV. The temperature dependences of the magnetic susceptibility, heat capacity and entropy have been satisfactorily described within the proposed model as well. Further INS investigations extended to higher incident neutron energies are necessary to verify the positions of the Γ_2 and $\Gamma_1^{(2)}$ levels predicted in our model at about 170 and 200 meV, respectively.

Acknowledgments

The author would like to thank Professor R Troć, Professor J Mulak and Dr D Kaczorowski for helpful and inspiring discussions and for their suggestions during preparation of the manuscript.

The author is also grateful to the referee for constructive suggestions for reorganizing this paper.

Appendix

The usual CF parameters can be obtained from the SM ones using the relation:

$$B_{kq} = \sum_t C^*_{kq}(\theta_t, \phi_t) b^t_k \tag{A1}$$

where t runs over ligands and, differently from (1) and (6), the spherical harmonics are functions of angular coordinates θ_t and ϕ_t of ligand t in the central coordinate system. Evaluating the geometrical factors $C^*_{kq}(\theta_t, \phi_t)$ in (A1) and making use of equations (7) one obtains for UOS

$$\begin{aligned}
B_{20} &= -0.041e^O_\sigma - 0.061e^O_\pi - 0.223e^S_\sigma - 0.364e^S_\pi \\
B_{40} &= -1.957e^O_\sigma - 0.652e^O_\pi + 4.566e^O_\delta + 0.969e^S_\sigma + 0.314e^S_\pi - 2.157e^S_\delta \\
B_{44} &= 1.230e^O_\sigma + 0.410e^O_\pi - 2.869e^O_\delta - 2.069e^S_\sigma - 0.693e^S_\pi + 4.868e^S_\delta \\
B_{60} &= 1.771e^O_\sigma - 2.657e^O_\pi + 1.063e^O_\delta + 3.547e^S_\sigma - 5.278e^S_\pi + 2.100e^S_\delta \\
B_{64} &= 3.052e^O_\sigma - 4.578e^O_\pi + 1.831e^O_\delta - 0.887e^S_\sigma + 1.337e^S_\pi - 0.537e^S_\delta
\end{aligned} \tag{A2}$$

for UOSe

$$\begin{aligned}
B_{20} &= -0.082e^O_\sigma - 0.123e^O_\pi - 0.122e^{Se}_\sigma - 0.196e^{Se}_\pi \\
B_{40} &= -1.910e^O_\sigma - 0.637e^O_\pi + 4.456e^O_\delta + 0.405e^{Se}_\sigma + 0.131e^{Se}_\pi - 0.935e^{Se}_\delta \\
B_{44} &= 1.265e^O_\sigma + 0.422e^O_\pi - 2.951e^O_\delta - 1.929e^{Se}_\sigma - 0.644e^{Se}_\pi + 4.504e^{Se}_\delta \\
B_{60} &= 1.885e^O_\sigma - 2.827e^O_\pi + 1.131e^O_\delta + 3.920e^{Se}_\sigma - 5.862e^{Se}_\pi + 2.349e^{Se}_\delta \\
B_{64} &= 3.010e^O_\sigma - 4.515e^O_\pi + 1.806e^O_\delta - 1.580e^{Se}_\sigma + 2.375e^{Se}_\pi - 0.949e^{Se}_\delta
\end{aligned} \tag{A3}$$

and for UOTe

$$\begin{aligned}
B_{20} &= -0.192e^O_\sigma - 0.287e^O_\pi - 0.156e^{Te}_\sigma - 0.291e^{Te}_\pi \\
B_{40} &= -1.764e^O_\sigma - 0.588e^O_\pi + 4.115e^O_\delta - 0.546e^{Te}_\sigma - 0.206e^{Te}_\pi + 1.368e^{Te}_\delta \\
B_{44} &= 1.361e^O_\sigma + 0.454e^O_\pi - 3.175e^O_\delta - 1.839e^{Te}_\sigma - 0.619e^{Te}_\pi + 4.317e^{Te}_\delta \\
B_{60} &= 2.144e^O_\sigma - 3.216e^O_\pi + 1.287e^O_\delta + 3.795e^{Te}_\sigma - 5.609e^{Te}_\pi + 2.258e^{Te}_\delta \\
B_{64} &= 2.868e^O_\sigma - 4.302e^O_\pi + 1.721e^O_\delta - 2.405e^{Te}_\sigma + 3.644e^{Te}_\pi - 1.451e^{Te}_\delta.
\end{aligned} \tag{A4}$$

The parameters e^Y_μ in equations (A2)–(A4) are defined for the average U–Y distance in UOY. The corresponding numerical coefficients have been evaluated using the ratios $e^{Y(1)}_\mu / e^{Y(2)}_\mu$ of the parameters taken from table 3.

The above relations need to be more simplified if they are to be applied in practice. This can be done in several ways. For example taking the following ratios of the AOM parameters determined from the *ab initio* calculations for UOS,

$$e^S_\sigma / e^O_\sigma = 0.619 \qquad e^S_\pi / e^O_\pi = 0.456 \qquad e^S_\delta / e^O_\delta = 0.511$$

simplifies (A2) to:

$$\begin{aligned}
B_{20} &= -0.228e_\sigma - 0.326e_\pi \\
B_{40} &= -1.720e_\sigma - 0.730e_\pi + 4.758e_\delta \\
B_{44} &= -0.066e_\sigma + 0.135e_\pi - 0.527e_\delta \\
B_{60} &= 5.032e_\sigma - 7.256e_\pi + 2.932e_\delta \\
B_{64} &= 3.174e_\sigma - 5.689e_\pi + 2.139e_\delta
\end{aligned} \tag{A5}$$

where $e_\mu \equiv (4e^O_\mu + 5e^S_\mu)/9$ are the averaged AOM parameters.

References

[1] Trzebiatowski W, Niemiec J and Sepichowska A 1961 *Bull Acad. Pol. Sci. Ser. Sci. Chim.* **9** 61
[2] Murasik A, Suski W, Troć R and Lejciejewicz J 1968 *Phys. Status Solidi* **30** 61
[3] Murasik A, Suski W and Lejciejewicz J 1969 *Phys. Status Solidi* **34** K157
[4] Larroque J, Chipaux R and Beauvy M 1986 *J. Less-Common Met.* **121** 487
[5] Amoretti G, Blaise A, Burlet P, Gordon J E and Troć R 1986 *J. Less-Common Met.* **121** 233
[6] Amoretti G, Blaise A, Bogé M, Bonnisseau D, Burlet P, Collard J M, Furnier J M, Quézel S, Rossat-Mignod J and Larroque J 1989 *J. Magn. Magn. Mater.* **79** 207
[7] Kaczorowski D, Pöttgen R, Gajek Z, Zygmunt A and Jeitschko W 1993 *J. Phys. Chem. Solids* **54** 723
[8] Sato N, Masuda H, Wakeshima M, Yamada K and Fujino T 1998 *J. Alloys Compounds* **265** 115
[9] Troć R and Zołnierek Z 1979 *J. Physique* **40** C4 79
[10] Troc R 1987 *Inorg. Chem. Acta.* **140** 67
[11] Amoretti G, Blaise A, Bonnet M, Caciuffo R, Erdös P, Noël H and Santini P 1995 *J. Magn. Magn. Mater.* **139** 339
[12] Amoretti G, Blaise A, Collard J M, Hall R O A, Mortimer M J and Troć R 1984 *J. Magn. Magn. Mater.* **46** 57
[13] Amoretti G, Blaise A, Caciuffo R, Furnier J M, Larroque J and Osborn R 1989 *J. Phys.: Condens. Matter* **1** 5711
[14] Dudarev S L, Manh Nguyen D and Sutton A P 1997 *Phil. Mag.* B **75** 613
[15] Shylk L, Troć R and Kaczorowski D 1995 *J. Magn. Magn. Mater.* **140–144** 1435
[16] Santini P, Lemański R and Erdös P 1999 *Adv. Phys.* **48** 537
[17] Gajek Z and Mulak J 1985 *Abstracts of 5th Int. Conf. on Crystalline Field and Anomalous Mixing Effects in f-Electron Systems (Senday, 1985)*
[18] Gajek Z, Lahalle M P, Krupa J C and Mulak J 1988 *J. Less-Common Met.* **124** 351
[19] Gajek Z, Mulak J and Faucher M 1987 *J. Phys. Chem. Solids* **48** 947
[20] Gajek Z 1995 *J. Alloys Compounds* **219** 238
[21] Goodman G L 1992 *J. Alloys Compound* **181** 33
[22] Divis M and Kuriplach J 1995 *Physica* B **205** 353
[23] Gerloch M, Harding J H and Wooley G 1981 *Struct. Bonding* **46** 1
[24] Amoretti G, Blaise A, Furnier J M, Caciuffo R, Larroque J, Osborn R, Taylor A D and Bowden Z A 1988 *J. Magn. Magn. Mater.* **76/77** 432
[25] Newman D J 1971 *Adv. Phys.* **20** 197
[26] Garcia D and Faucher M 1985 *J. Chem. Phys.* **82** 5554
[27] Schmidt P C, Weiss A and Das T P 1979 *Phys. Rev.* B **19** 5525
[28] Erdös P and Robinson J 1983 *The Physics of Actinide Compounds* (New York: Plenum)
[29] Gajek Z and Mulak J 1992 *J. Phys.: Condens. Matter* **4** 427
[30] Newman D J 1983 *J. Phys. F: Met. Phys.* **13** 1511
[31] Dixon J M and Wardlaw R S 1986 *Physica* A **135** 105
[32] Shen Y R and Holzapfel W B 1994 *J. Phys.: Condens. Matter* **6** 2367
[33] Gajek Z, Krupa J C and Antic-Fidancev E 1997 *J. Phys.: Condens. Matter* **9** 557
[34] Kaczorowski D 1999 private communication
[35] Birgeneau R J 1972 *J. Phys. Chem. Solids* **33** 59
[36] Amoretti G, Blaise A, Caciuffo R, Furnier J M, Hutchings M T, Osborn R and Taylor A D 1989 *Phys. Rev.* B **40** 1856
[37] Troć R 1999 private communication